CMS Physics Analysis Summary

Contact: cms-pag-conveners-heavyions@cern.ch 2017/08/21

Comparison of jet fragmentation for isolated-photon+jet pairs in PbPb and pp collisions at $\sqrt{s_{\mathrm{NN}}} = 5.02$ TeV

The CMS Collaboration

Abstract

Measurements of fragmentation functions for jets paired with an isolated photon in pp and, for the first time, PbPb collisions are presented. The analysis uses data from the CMS detector at the CERN LHC, with both systems at a nucleon-nucleon center-of-mass energy of 5.02 TeV. Fragmentation functions are constructed using charged particles with transverse momentum $p_{\mathrm{T}}^{\mathrm{trk}} > 1\,\mathrm{GeV}/c$ inside jets with transverse momentum $p_{\mathrm{T}}^{\mathrm{jet}} > 30\,\mathrm{GeV}/c$ for events containing an isolated photon with $p_{\mathrm{T}}^{\gamma} > 60\,\mathrm{GeV}/c$. For central PbPb collisions, modifications of the jet fragmentation function with respect to that found for pp collisions are observed, while no significant differences are found in the 50% most peripheral collisions. The modifications seen in central events indicate an enhancement for particles at low p_{T} and a depletion at high p_{T}, with a transition around $3\,\mathrm{GeV}/c$. These measurements provide information about the longitudinal modifications of a parton shower whose initial kinematics are tightly constrained by the properties of the associated photon.

A deconfined state of quarks and gluons, called the quark-gluon plasma (QGP) [1], can be produced over a very short timescale, $\tau \approx 1\,\mathrm{fm}/c$, in high energy nucleus-nucleus collisions [2]. Occasionally, a pair of quarks and/or gluons in the colliding nuclei will undergo a high transverse momentum scattering, a process that occurs over a similarly short timescale. As they pass through and interact with the QGP, losing some of their energy in the process, the outgoing partons from such an interaction act as tomographic probes of the medium [3–8]. Understanding how these partons lose energy, whether by heating the medium or by scattering off point-like constituents of the QGP, has been a main focus of the field of relativistic heavy ion collisions.

Jets, collimated energy deposits from particles that originated from a single high-momentum parton, can be measured experimentally. The LHC collaborations have measured various properties of jets and dijet pairs such as the momentum dependence of jet energy loss in the medium, also known as "jet quenching" [9–11], jet fragmentation functions [12, 13], missing transverse momentum (p_{T}) in dijet systems [14–16], and jet-track correlations [17]. However, understanding how properties of the measured jets relate to their parent partons is one of the challenges of these measurements. When selecting events based solely on jet kinematics, it is impossible to control the initial configuration of the partons, since the amount of energy lost to the medium before forming the final-state particles comprising the jet cannot be unambiguously determined. One way to overcome this challenge is to study the rare processes where one of the partons from the initial hard scattering is a high energy reconstructable electroweak boson, namely a photon or a Z boson. Since electroweak bosons do not experience any quantum chromodynamic interactions, they are largely unaffected by their passage through the QGP, and their measured kinematics should be very close to those just after the initial hard scattering. As a result, a jet sample tagged with the presence of a high p_{T} photon or Z boson should have well-defined initial configurations and, therefore, will allow more constrained jet studies and comparisons with theoretical calculations. Photon studies only include those that are "isolated", i.e. not surrounded by any significant energy, in order to eliminate dijet events in which a high-p_{T} photon originates from one of the jets.

The CMS Collaboration has previously measured the azimuthal correlation and momentum imbalance of isolated-photon+jet pairs in pp and PbPb at a nucleon-nucleon center-of-mass energy $\sqrt{s_{\mathrm{NN}}} = 2.76\,\mathrm{TeV}$ [18] and of Z+jet pairs at $\sqrt{s_{\mathrm{NN}}} = 5.02\,\mathrm{TeV}$ [19]. This paper presents the first measurement of the fragmentation function of jets associated with an isolated photon. The analysis uses PbPb and pp data at $\sqrt{s_{\mathrm{NN}}} = 5.02\,\mathrm{TeV}$ collected in 2015 and corresponding to integrated luminosities of $404\,\mu\mathrm{b}^{-1}$ and $27.4\,\mathrm{pb}^{-1}$, respectively. The results from PbPb and pp collisions are compared in order to search for modifications due to the presence of the QGP.

The central feature of CMS is a superconducting solenoid of 6 m internal diameter, providing a magnetic field of 3.8 T. Within the solenoid volume are a silicon pixel and strip tracker, a lead tungstate crystal electromagnetic calorimeter (ECAL), and a brass and scintillator hadron calorimeter (HCAL), each composed of a barrel and two endcap sections. Forward hadron (HF) calorimeters extend the pseudorapidity (η) coverage and are used for event selection, and in the case of PbPb events, also to determine the degree of overlap ("centrality") of the two colliding Pb nuclei [15] and the event-by-event azimuthal angle of maximum particle density ("event plane") [20]. Muons are detected in gas-ionization chambers embedded in the steel flux-return yoke outside the solenoid. A more detailed description of the CMS detector, together with a definition of the coordinate system used and the relevant kinematic variables, can be found in Ref. [21].

The event samples are selected online with dedicated photon triggers [22], and cleaned offline to remove noncollision events, such as beam-gas interactions or cosmic-ray muons [23]. In ad-

dition, events are required to have a primary vertex reconstructed within 15 cm of the nominal interaction point along the beam direction and within 0.15 cm of the nominal interaction point in the transverse plane. Offline, the same reconstruction algorithms, analysis selections, and energy scales and resolution corrections are used for jets and photons as in Ref. [22]. For the analysis of PbPb collisions, the event centrality is defined as the fraction of the total inelastic hadronic cross section, starting at 0% for the most central collisions and evaluated as percentiles of the distribution of the energy deposited in the HF [15]. The results are presented in four centrality intervals: the most central 0–10% (i.e. the 10% having the largest overlap area of the two nuclei), two intermediate intervals 10–30% and 30–50%, and a peripheral 50-100% category (i.e. the most pp-like environment).

Photon candidates are reconstructed from clusters of energy deposited in the ECAL [24, 25]. Electron contamination and anomalous signals caused by the interaction of heavily-ionising particles directly with the silicon avalanche photodiodes used for the ECAL barrel readout are removed as described in Ref. [25]. The photon candidates used in this analysis are restricted to be in the barrel region of the ECAL, $|\eta^{\gamma}| < 1.44$, and required to have $p_{\mathrm{T}}^{\gamma} > 60\,\mathrm{GeV}/c$. This p_{T}^{γ} threshold is used so that more quenched jets (i.e. cases where the parton associated with the photon lost considerable energy) would be above the minimum $p_{\mathrm{T}}^{\mathrm{jet}}$ threshold discussed later. A sample enriched in prompt photons (i.e. ones produced directly in the initial hard scattering) is obtained using the same requirements as in Refs. [22, 25]. The strategy is to limit the additional energy in a cone of fixed radius $\Delta R = \sqrt{(\Delta\eta)^2 + (\Delta\phi)^2} = 0.4$ around the reconstructed photon. This restriction suppresses the background contributions from photons directly produced in parton-fragmentation and from decays of hadrons produced in fragmentation, and it yields so-called "isolated photons" which consist mostly of prompt photons. The dominant remaining backgrounds for isolated photon candidates are ECAL showers initiated by isolated hadrons, and real photons that are decay products of isolated neutral mesons, e.g. π^0, η, and ω. As in Refs. [25, 26], the hadron-induced showers are rejected using the ratio of HCAL over ECAL energy inside a cone of radius $\Delta R = 0.15$ around the photon candidate, and decay photons are significantly reduced using a cut on the shower shape, a measure of how energy deposited in the ECAL is distributed in ϕ and η. Finally, the photon purity, the fraction of prompt photons within the remaining collection of isolated photon candidates, is extracted in a data-driven way using a template fit of the shower shape as detailed in Refs. [18, 22].

The energy of the reconstructed photons is corrected to account for the effects of the material in front of the ECAL and incomplete containment of the shower energy. An additional correction is applied in PbPb collisions to account for energy contamination from the underlying PbPb event (UE). The size of the resulting energy correction for isolated photons varies from 0 to 10%, depending on p_{T}^{γ} and the centrality of the collision. The corrections are obtained using simulated photon events from the PYTHIA 8.212 [27] (CUETP8M1 tune [28]) Monte Carlo (MC) event generator which are embedded into simulated background events using HYDJET [29] (Cymbal5Ev8 tune), which was tuned to reproduce the observed charged particle multiplicity and p_{T} spectrum in PbPb data.

The particle-flow (PF) algorithm [30] is deployed for the reconstruction of the jets used in this analysis. By combining information from all sub-detector systems, the PF algorithm identifies stable particles in an event, classifying them as electrons, muons, photons, charged and neutral hadrons. To form jets, those PF objects are clustered using the anti-k_{T} sequential recombination algorithm provided in the FASTJET framework [31, 32], with a size parameter of $R = 0.3$. In order to subtract the UE background in PbPb collisions, the iterative algorithm explained in Ref. [33], using the same implementation as in Refs. [15, 18, 34], is employed. In pp collisions, jets are reconstructed without UE subtraction. The jet energy corrections are derived from

simulation, and are confirmed via energy balance methods applied to dijet and photon+jet events in pp data [35]. Jets with $|\eta^{\mathrm{jet}}| < 1.6$ and corrected $p_{\mathrm{T}}^{\mathrm{jet}} > 30\,\mathrm{GeV}/c$ are selected for this analysis. Simulation studies show that the jet selection efficiency and energy resolution are well understood in this kinematic range.

In each event, photon+jet pairs are formed by associating the highest p_{T}^{γ} isolated photon candidate passing the selection criteria with all jets in the same event that pass the jet selection. Furthermore, an azimuthal separation of $\Delta\phi_{j\gamma} = |\phi^{\mathrm{jet}} - \phi^{\gamma}| > 7\pi/8$ is required of the photon+jet pairs to suppress the contributions from background jets and photon+multijet events. Charged particle tracks are combined with the selected jet and photon to measure the fragmentation functions. For both pp and PbPb data, the selection criteria, as well as the corrections for tracking efficiency, detector acceptance, and misreconstruction rate, are the same as in Ref. [23]. The tracks used in this analysis are required to have $p_{\mathrm{T}}^{\mathrm{trk}} > 1\,\mathrm{GeV}/c$ and fall within the jet cone, i.e., $\Delta R \leq 0.3$.

To study the correlation of the photon, jets, and charged particles produced in the same scattering in PbPb collisions, the following combinatorial backgrounds must be subtracted: misidentified jets resulting from UE fluctuations, jets from multiple hard parton-parton scatterings in the same collision, and tracks from the UE that fall within the cone of the selected jet. The two backgrounds from jets are estimated following the same procedure as in Refs. [18, 22]. Each leading isolated photon candidate is correlated with jets found in different events that are chosen randomly from a set of minimum bias PbPb data with similar event centrality, interaction vertex position, and event plane angle. The background contribution from tracks from the UE is estimated using a data-driven method which correlates each selected jet in the signal event with tracks found in different events, also selected randomly as described above. In order to compare results from PbPb collisions to pp reference data, the jet energy in pp events is smeared, i.e. convoluted with a Gaussian resolution adjustment term, to match the jet energy resolution in each of the PbPb centrality intervals in which the comparison is made [22]. The background contribution from the pairing of decay photons with jets is accounted for using the photon purity found from the shower shape fits discussed previously.

After correcting for the contributions from decay photons and the combinatorial background of jets and charged particles, the photon-tagged fragmentation functions are presented as distributions of $\xi^{\mathrm{jet}} = \ln \frac{|\mathbf{p}^{\mathrm{jet}}|^2}{\mathbf{p}^{\mathrm{trk}} \cdot \mathbf{p}^{\mathrm{jet}}}$ and $\xi_{\mathrm{T}}^{\gamma} = \ln \frac{-|\mathbf{p}_{\mathrm{T}}^{\gamma}|^2}{\mathbf{p}_{\mathrm{T}}^{\mathrm{trk}} \cdot \mathbf{p}_{\mathrm{T}}^{\gamma}}$, where $\mathbf{p}^{\mathrm{jet}}$ and $\mathbf{p}^{\mathrm{trk}}$ are the 3-momenta of the jet and charged-particle, and $\mathbf{p}_{\mathrm{T}}^{\gamma}$ and $\mathbf{p}_{\mathrm{T}}^{\mathrm{trk}}$ are the transverse components of the photon and charged-particle 3-momenta. These variables provide information about the longitudinal distribution of jet energy inside the jet cone and hence, the fragmentation pattern of jets [36]. While ξ^{jet} gives the fragmentation pattern with respect to the energy of a reconstructed jet, $\xi_{\mathrm{T}}^{\gamma}$ stands as a proxy for the fragmentation pattern with respect to the energy of the initial parton.

Multiple sources of systematic uncertainty are considered for the ξ^{jet} and $\xi_{\mathrm{T}}^{\gamma}$ results, including photon purity, photon energy scale, photon isolation, electron contamination, jet energy scale, jet energy resolution, tracking efficiency, and UE background. The total uncertainty is calculated by summing in quadrature the uncertainties from all sources. The following systematic uncertainties represent an average over all ξ^{jet} and $\xi_{\mathrm{T}}^{\gamma}$ bins, and in the case of PbPb results are quoted only for the most challenging case, the one with 0–10% event centrality. The same procedures as in Ref. [22] are applied in this analysis to evaluate the systematic uncertainties related to the isolated photons used. The uncertainty in the photon purity estimation is evaluated by varying components of the shower shape template. The maximum variations with respect to the nominal case are propagated as systematic uncertainties, amounting to 4.1%

(7.5%) for the 0–10% most central events, and 0.5% (0.5%) for pp results, for ξ^{jet} ($\xi_{\mathrm{T}}^{\gamma}$). The total systematic uncertainty resulting from the experimental criterion for an isolated photon is 2.2% (1.1%) and 0.9% (0.8%) for ξ^{jet} ($\xi_{\mathrm{T}}^{\gamma}$), for PbPb and pp, respectively. The residual data-to-MC photon energy scale difference after applying the photon energy corrections is also quoted as a systematic uncertainty of 1.9% (2.4%) and $< 0.1\%$ for ξ^{jet} ($\xi_{\mathrm{T}}^{\gamma}$), for PbPb and pp, respectively. The amount of electron contamination in the samples is determined to be around 5% (14%) after (before) any rejection is applies. An uncertainty is evaluated by repeating the analysis without applying electron rejection, and scaling the difference in the final observables to the residual electron contamination after applying electron rejection, giving 1.8% (1.7%) and 0.4% (0.3%) for ξ^{jet} ($\xi_{\mathrm{T}}^{\gamma}$), for PbPb and pp, respectively. The uncertainties related to the jet energy resolution and jet energy scale are the same as in Ref. [22]. When propagated into the present results, the uncertainty related to the jet energy scale amounts to 8.0% (5.7%) and 2.8% (0.2%) for ξ^{jet} ($\xi_{\mathrm{T}}^{\gamma}$), in the PbPb and pp cases, respectively, while the energy resolution gives uncertainties of 5.3% (2.4%) and 1.3% (0.5%) for ξ^{jet} ($\xi_{\mathrm{T}}^{\gamma}$), for PbPb and pp, respectively. A systematic uncertainty is assigned to account for long-range η correlations [17] that contribute to the UE. It is estimated by constructing the observables using tracks lying within the same azimuthal angle as the jet, but separated by a large pseudorapidity interval, $1.5 < \Delta\eta < 2.4$. It is found to be 4.7% (3.5%) and 1.5% (1.4%) for ξ^{jet} ($\xi_{\mathrm{T}}^{\gamma}$), for PbPb and pp, respectively. The uncertainty related to the tracking inefficiency is estimated as the difference in the track reconstruction efficiency between data and MC [23]. It is 5% (4%) for PbPb (pp) results, and flat as a function of the track p_{T} and event centrality.

For PbPb results only, two additional sources of systematic uncertainties are considered. One is for the background subtraction method, and is estimated using an alternative background subtraction procedure, the so-called η-reflection method [12]. The assigned uncertainty is 3.4% for ξ^{jet} and $\xi_{\mathrm{T}}^{\gamma}$. The other uncertainty accounts for differences in the jet energy response due to ξ^{jet} and $\xi_{\mathrm{T}}^{\gamma}$ variances in the jet fragmentation pattern, as observed in simulation. The full maximum observed differences of 17% for $\xi^{\mathrm{jet}} < 1$ and 9.7% (11.1%) for $\xi^{\mathrm{jet}}(\xi_{\mathrm{T}}^{\gamma}) > 2.5$ are propagated as uncertainties in the corresponding ξ^{jet} and $\xi_{\mathrm{T}}^{\gamma}$ regions for the PbPb results.

Figure 1 shows the photon-tagged fragmentation functions as a function of ξ^{jet} for both PbPb and pp collisions, together with the ratio of the PbPb to pp distributions.The ξ^{jet} distributions in PbPb collisions represent the fragmentation pattern of a jet that may have lost energy through interactions with the medium, while the fragmentation function measured in pp collisions represents the fragmentation pattern of unquenched jets. However, it should be kept in mind that the collection of jets in PbPb and pp collisions are not necessarily equivalent, since the samples are selected based on the photon energy. The ξ^{jet} distributions in 50–100% PbPb collisions are consistent with those in pp collisions. In more central collisions, an enhancement of the fragmentation function in PbPb collisions with respect to the reference pp data is observed for $\xi^{\mathrm{jet}} > 2.5$ region (corresponding to $p_{\mathrm{T}}^{\mathrm{trk}} \lesssim 2.5\,\mathrm{GeV}/c$ for $p_{\mathrm{T}}^{\mathrm{jet}} = 30\,\mathrm{GeV}/c$ and $\Delta R = 0$ between the track and the jet), indicating that there is a small excess of soft particles within the jet cone. The magnitude of the enhancement increases with increasing event centrality. Additionally, a slight suppression of the fragmentation function in the region $0.5 < \xi^{\mathrm{jet}} < 2.5$ (corresponding to $18 \gtrsim p_{\mathrm{T}}^{\mathrm{trk}} \gtrsim 2.5\,\mathrm{GeV}/c$ for $p_{\mathrm{T}}^{\mathrm{jet}} = 30\,\mathrm{GeV}/c$ and $\Delta R = 0$ between the track and the jet) is also observed in the most central PbPb collisions when compared to pp collisions.

Figure 2 shows the photon-tagged fragmentation functions as a function of $\xi_{\mathrm{T}}^{\gamma}$ for PbPb and pp collisions, as well as their ratio, in four event centrality intervals. In peripheral PbPb collisions, the $\xi_{\mathrm{T}}^{\gamma}$ distributions are consistent with those in pp collisions. As the collisions become more central, an enhancement in the $\xi_{\mathrm{T}}^{\gamma} > 3$ region (corresponding to $p_{\mathrm{T}}^{\mathrm{trk}} \lesssim 3\,\mathrm{GeV}/c$ for $p_{\mathrm{T}}^{\gamma} = 60\,\mathrm{GeV}/c$ and $\Delta\phi = \pi$ between the track and the photon) relative to pp collisions is ob-

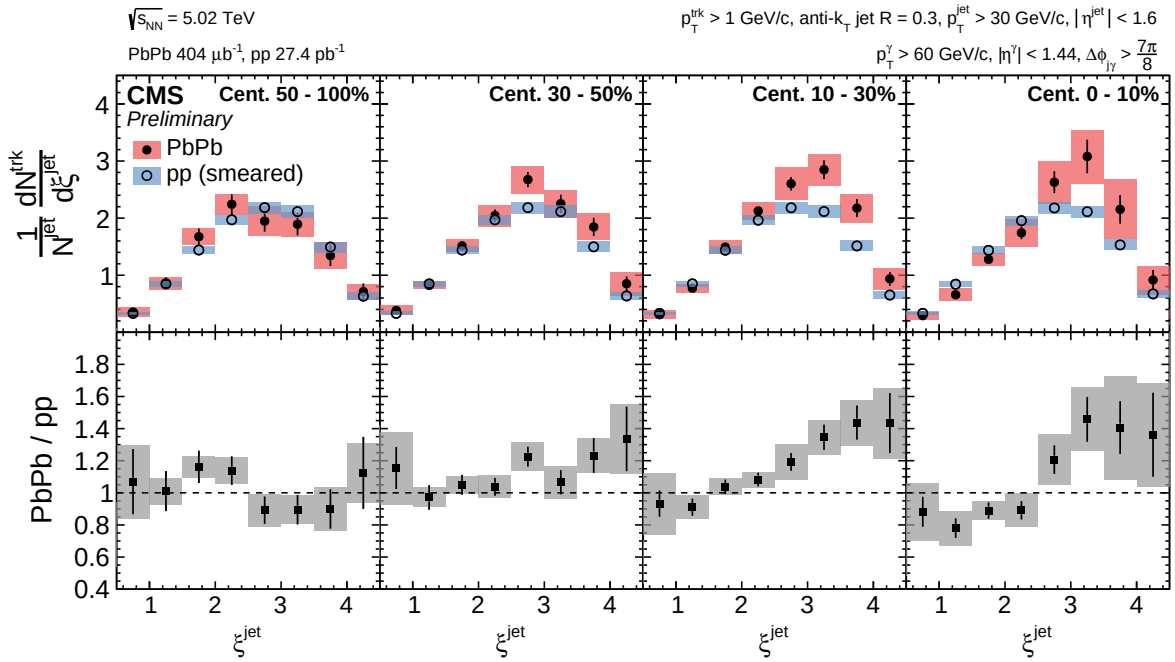

Figure 1: **Top:** The centrality dependence of the ξ^{jet} distribution for jets associated with an isolated photon for PbPb (full markers) and pp (open markers) collisions. **Bottom:** The ratios of the PbPb to pp distributions. The vertical lines through the points represent statistical uncertainties, while the colored boxes indicate the systematic uncertainties.

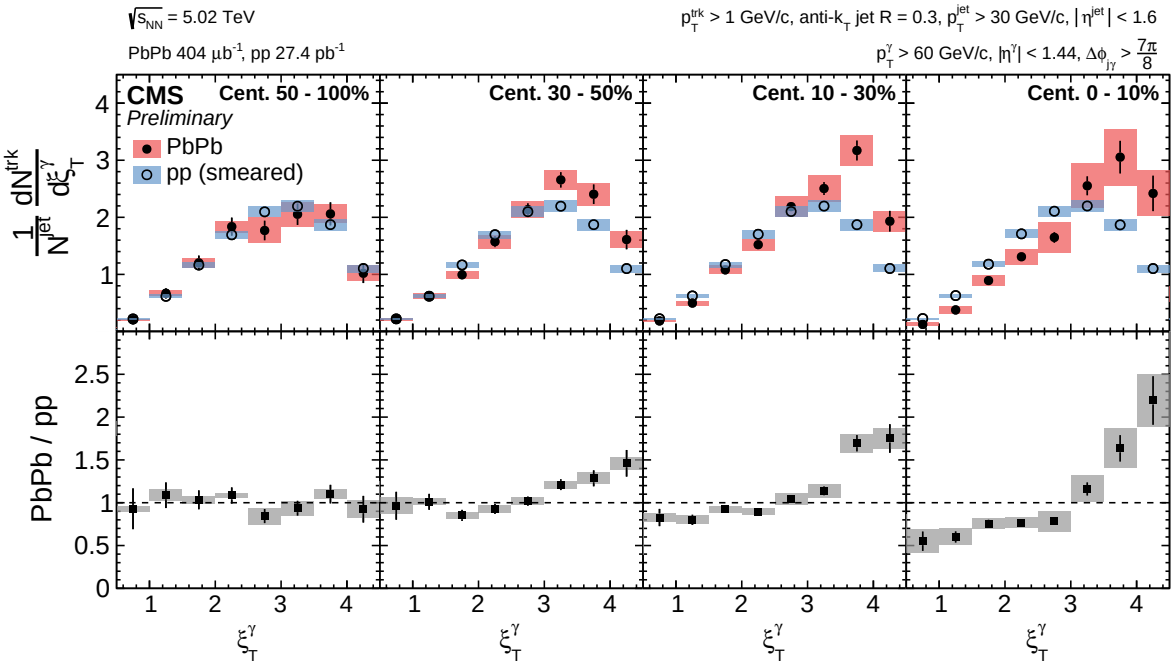

Figure 2: **Top:** The centrality dependence of the $\xi_{\mathrm{T}}^{\gamma}$ distribution for jets associated with an isolated photon for PbPb (full markers) and pp (open markers) collisions. **Bottom:** The ratios of the PbPb to pp distributions. The vertical lines through the points represent statistical uncertainties, while the colored boxes indicate the systematic uncertainties.

served in PbPb collisions. The magnitude of this enhancement increases with increasing event centrality, and is more pronounced than the enhancement observed in the ξ^{jet} distributions. A clear suppression of the $\xi_{\mathrm{T}}^{\gamma}$ distribution is also observed for $0.5 < \xi_{\mathrm{T}}^{\gamma} < 3$ region (corresponding to $36 \gtrsim p_{\mathrm{T}}^{\mathrm{trk}} \gtrsim 3\,\mathrm{GeV}/c$ for $p_{\mathrm{T}}^{\gamma} = 60\,\mathrm{GeV}/c$ and $\Delta\phi = \pi$ between the track and the photon) in the most central PbPb collisions as compared to pp collisions. This pattern of suppression and enhancement is direct evidence of the energy loss experienced by high p_{T} partons as they traverse the high density medium created in heavy ion collisions.

The enhancement at large ξ^{jet} and $\xi_{\mathrm{T}}^{\gamma}$, together with the suppression at low ξ^{jet} and $\xi_{\mathrm{T}}^{\gamma}$, support the picture that the showers of partons that traversed the medium contain relatively more particles with lower energy and relatively fewer particles with high energy. The stronger enhancements and suppressions observed in the $\xi_{\mathrm{T}}^{\gamma}$ distributions as compared to ξ^{jet} show that the modification of fragmentation patterns measured using initial parton energy is more pronounced than the one measured using detector-level jet energy. Qualitatively, this is not surprising. First, a shift to lower values between the ξ^{jet} and $\xi_{\mathrm{T}}^{\gamma}$ distributions is also observed in the pp results, because of effects such as out-of-cone radiation not being captured in the $\Delta R = 0.3$ jet area used in this analysis. Then, in PbPb collisions, a similar shift happens if the jet is quenched: the jet momentum is lower than that of the parton, resulting in a shift to lower ξ^{jet}. As a result, the modifications in the ratio PbPb/pp are weakened by quenching in the case of ξ^{jet}, and are more pronounced in the $\xi_{\mathrm{T}}^{\gamma}$ case.

In summary, the fragmentation functions of jets associated with isolated photons are presented in pp and, for the first time, in PbPb collisions at $\sqrt{s_{\mathrm{NN}}} = 5.02\,\mathrm{TeV}$. The fragmentation functions are constructed for jets with $p_{\mathrm{T}}^{\mathrm{jet}} > 30\,\mathrm{GeV}/c$ and charged particles with $p_{\mathrm{T}}^{\mathrm{trk}} > 1\,\mathrm{GeV}/c$ that are associated with an isolated photon with $p_{\mathrm{T}}^{\gamma} > 60\,\mathrm{GeV}/c$, and are studied as functions of ξ^{jet} and $\xi_{\mathrm{T}}^{\gamma}$, in four different PbPb event centrality intervals. The modifications of the ξ^{jet} and $\xi_{\mathrm{T}}^{\gamma}$ distributions in central PbPb collisions indicate that there is an excess of low energy particles and a depletion of high energy particles inside the jet. This picture is more apparent in the $\xi_{\mathrm{T}}^{\gamma}$ distributions, where the photon-based selection allows for the tagging of the initial parton kinematics (before the quenching happened). The association with isolated photons provides, for the first time, information on the medium modification of parton showers in events with well-defined initial parton kinematics.

References

[1] F. Karsch, "The Phase transition to the quark gluon plasma: Recent results from lattice calculations", *Nucl. Phys. A* **590** (1995) 367C, doi:10.1016/0375-9474(95)00248-Y, arXiv:hep-lat/9503010.

[2] J. D. Bjorken, "Highly relativistic nucleus-nucleus collisions: The central rapidity region", *Phys. Rev. D* **27** (1983) 140, doi:10.1103/PhysRevD.27.140.

[3] D. A. Appel, "Jets as a probe of quark-gluon plasmas", *Phys. Rev. D* **33** (1986) 717, doi:10.1103/PhysRevD.33.717.

[4] J. Blaizot and L. D. McLerran, "Jets in Expanding Quark - Gluon Plasmas", *Phys. Rev. D* **34** (1986) 2739, doi:10.1103/PhysRevD.34.2739.

[5] M. Gyulassy and M. Plumer, "Jet Quenching in Dense Matter", *Phys. Lett. B* **243** (1990) 432, doi:10.1016/0370-2693(90)91409-5.

[6] X.-N. Wang and M. Gyulassy, "Gluon shadowing and jet quenching in $A + A$ collisions at $\sqrt{s} = 200A$ GeV", *Phys. Rev. Lett.* **68** (1992) 1480, doi:10.1103/PhysRevLett.68.1480.

[7] R. Baier et al., "Radiative energy loss and p(T) broadening of high-energy partons in nuclei", *Nucl. Phys. B* **484** (1997) 265, doi:10.1016/S0550-3213(96)00581-0, arXiv:hep-ph/9608322.

[8] B. Zakharov, "Radiative energy loss of high-energy quarks in finite size nuclear matter and quark - gluon plasma", *JETP Lett.* **65** (1997) 615, doi:10.1134/1.567389, arXiv:hep-ph/9704255.

[9] ATLAS Collaboration, "Measurements of the Nuclear Modification Factor for Jets in Pb+Pb Collisions at $\sqrt{s_{\rm NN}} = 2.76$ TeV with the ATLAS Detector", *Phys. Rev. Lett.* **114** (2015) 072302, doi:10.1103/PhysRevLett.114.072302, arXiv:1411.2357.

[10] ALICE Collaboration, "Measurement of jet suppression in central Pb-Pb collisions at $\sqrt{s_{\rm NN}}$ = 2.76 TeV", *Phys. Lett. B* **746** (2015) 1, doi:10.1016/j.physletb.2015.04.039, arXiv:1502.01689.

[11] CMS Collaboration, "Measurement of inclusive jet cross sections in pp and PbPb collisions at $\sqrt{s_{NN}} = 2.76$ TeV", *Phys. Rev. C* **96** (2017) 015202, doi:10.1103/PhysRevC.96.015202, arXiv:1609.05383.

[12] CMS Collaboration, "Measurement of jet fragmentation in PbPb and pp collisions at $\sqrt{s_{\rm NN}} = 2.76$ TeV", *Phys. Rev. C* **90** (2014) 024908, doi:10.1103/PhysRevC.90.024908, arXiv:1406.0932.

[13] ATLAS Collaboration, "Measurement of jet fragmentation in Pb+Pb and pp collisions at $\sqrt{s_{\rm NN}} = 2.76$ TeV with the ATLAS detector at the LHC", *Eur. Phys. J. C* **77** (2017) 379, doi:10.1140/epjc/s10052-017-4915-5, arXiv:1702.00674.

[14] ATLAS Collaboration, "Observation of a Centrality-Dependent Dijet Asymmetry in Lead-Lead Collisions at $\sqrt{s_{NN}} = 2.77$ TeV with the ATLAS Detector at the LHC", *Phys. Rev. Lett.* **105** (2010) 252303, doi:10.1103/PhysRevLett.105.252303, arXiv:1011.6182.

[15] CMS Collaboration, "Observation and studies of jet quenching in PbPb collisions at nucleon-nucleon center-of-mass energy = 2.76 TeV", *Phys. Rev. C* **84** (2011) 024906, doi:10.1103/PhysRevC.84.024906, arXiv:1102.1957.

[16] CMS Collaboration, "Measurement of transverse momentum relative to dijet systems in PbPb and pp collisions at $\sqrt{s_{\rm NN}} = 2.76$ TeV", *JHEP* **01** (2016) 006, doi:10.1007/JHEP01(2016)006, arXiv:1509.09029.

[17] CMS Collaboration, "Decomposing transverse momentum balance contributions for quenched jets in PbPb collisions at $\sqrt{s_{\rm NN}} = 2.76$ TeV", *JHEP* **11** (2016) 055, doi:10.1007/JHEP11(2016)055, arXiv:1609.02466.

[18] CMS Collaboration, "Studies of jet quenching using isolated-photon+jet correlations in PbPb and pp collisions at $\sqrt{s_{\rm NN}} = 2.76$ TeV", *Phys. Lett. B* **718** (2013) 773, doi:10.1016/j.physletb.2012.11.003, arXiv:1205.0206.

[19] CMS Collaboration, "Study of jet quenching with Z+jet correlations in PbPb and pp collisions at $\sqrt{s_{\rm NN}} = 5.02$ TeV", (2017). arXiv:1702.01060. Submitted to *Phys. Rev. Lett.*

[20] CMS Collaboration, "Azimuthal anisotropy of charged particles at high transverse momenta in PbPb collisions at $\sqrt{s_{\mathrm{NN}}} = 2.76$ TeV", *Phys. Rev. Lett.* **109** (2012) 022301, doi:10.1103/PhysRevLett.109.022301, arXiv:1204.1850.

[21] CMS Collaboration, "The CMS experiment at the CERN LHC", *JINST* **3** (2008) S08004, doi:10.1088/1748-0221/3/08/S08004.

[22] CMS Collaboration, "Study of Isolated-Photon + Jet Correlations in PbPb and pp Collisions at $\sqrt{s_{\mathrm{NN}}} = 5.02$ TeV", Technical Report CMS-PAS-HIN-16-002, CERN, Geneva, 2016.

[23] CMS Collaboration, "Charged-particle nuclear modification factors in PbPb and pPb collisions at $\sqrt{s_{\mathrm{NN}}} = 5.02$ TeV", *JHEP* **04** (2017) 039, doi:10.1007/JHEP04(2017)039, arXiv:1611.01664.

[24] CMS Collaboration, "Performance of photon reconstruction and identification with the CMS detector in proton-proton collisions at $\sqrt{s} = 8$ TeV", *JINST* **10** (2015) P08010, doi:10.1088/1748-0221/10/08/P08010, arXiv:1502.02702.

[25] CMS Collaboration, "Measurement of isolated photon production in pp and PbPb collisions at $\sqrt{s_{NN}} = 2.76$ TeV", *Phys. Lett. B* **710** (2012) 256, doi:10.1016/j.physletb.2012.02.077, arXiv:1201.3093.

[26] CMS Collaboration, "Measurement of the Isolated Prompt Photon Production Cross Section in pp Collisions at $\sqrt{s} = 7$ TeV", *Phys. Rev. Lett.* **106** (2011) 082001, doi:10.1103/PhysRevLett.106.082001, arXiv:1012.0799.

[27] T. Sjöstrand, S. Mrenna, and P. Z. Skands, "A brief introduction to PYTHIA 8.1", *Comput. Phys. Commun.* **178** (2008) 852, doi:10.1016/j.cpc.2008.01.036, arXiv:0710.3820.

[28] CMS Collaboration, "Event generator tunes obtained from underlying event and multiparton scattering measurements", *Eur. Phys. J. C* **76** (2016) 155, doi:10.1140/epjc/s10052-016-3988-x, arXiv:1512.00815.

[29] I. P. Lokhtin and A. M. Snigirev, "A model of jet quenching in ultrarelativistic heavy ion collisions and high-pT hadron spectra at RHIC", *Eur. Phys. J. C* **45** (2006) 211, doi:10.1140/epjc/s2005-02426-3, arXiv:hep-ph/0506189.

[30] CMS Collaboration, "Particle-flow reconstruction and global event description with the CMS detector", (2017). arXiv:1706.04965. Submitted to *JINST*.

[31] M. Cacciari, G. P. Salam, and G. Soyez, "The Anti-k(t) jet clustering algorithm", *JHEP* **04** (2008) 063, doi:10.1088/1126-6708/2008/04/063, arXiv:0802.1189.

[32] M. Cacciari, G. P. Salam, and G. Soyez, "FastJet User Manual", *Eur. Phys. J. C* **72** (2012) 1896, doi:10.1140/epjc/s10052-012-1896-2, arXiv:1111.6097.

[33] O. Kodolova, I. Vardanian, A. Nikitenko, and A. Oulianov, "The performance of the jet identification and reconstruction in heavy ions collisions with CMS detector", *Eur. Phys. J. C* **50** (2007) 117, doi:10.1140/epjc/s10052-007-0223-9.

[34] CMS Collaboration, "Jet momentum dependence of jet quenching in PbPb collisions at $\sqrt{s_{\mathrm{NN}}} = 2.76$ TeV", *Phys. Lett. B* **712** (2012) 176, doi:10.1016/j.physletb.2012.04.058, arXiv:1202.5022.

[35] CMS Collaboration, "Determination of Jet Energy Calibration and Transverse Momentum Resolution in CMS", *JINST* **6** (2011) P11002, doi:10.1088/1748-0221/6/11/P11002, arXiv:1107.4277.

[36] J. Casalderrey-Solana et al., "Predictions for Boson-Jet Observables and Fragmentation Function Ratios from a Hybrid Strong/Weak Coupling Model for Jet Quenching", *JHEP* **03** (2016) 053, doi:10.1007/JHEP03(2016)053, arXiv:1508.00815.